Journal of Controlled Release 220 (2015) 316–328

Contents lists available at ScienceDirect

Journal of Controlled Release

journal homepage: www.elsevier.com/locate/jconrel

Disarmed anthrax toxin delivers antisense oligonucleotides and siRNA with high efficiency and low toxicity

Paul D.R. Dyer [a,1], Thomas R. Shepherd [a,1], Alexander S. Gollings [a,1], Susan A. Shorter [a,1], Monique A.M. Gorringe-Pattrick [a], Chun-Kit Tang [a], Beatrice N. Cattoz [c], Les Baillie [b], Peter C. Griffiths [c], Simon C.W. Richardson [a,*]

[a] Intercellular Delivery Solutions Laboratory, Faculty of Engineering and Science, University of Greenwich, Central Avenue, Chatham Maritime, Kent, ME4 4TB, UK
[b] School of Pharmacy and Pharmaceutical Sciences, Cardiff University, King Edward VII Avenue, Cardiff CF10 3AX, UK
[c] Department of Pharmaceutical, Chemical and Environmental Science, Faculty of Engineering and Science, University of Greenwich, Central Avenue, Chatham Maritime, Kent ME4 4TB, UK

ARTICLE INFO

Article history:
Received 28 July 2015
Received in revised form 26 October 2015
Accepted 28 October 2015
Available online xxxx

Keywords:
Antisense
RNAi
Anthrax toxin
PEG-dilemma
Non-viral

ABSTRACT

Inefficient cytosolic delivery and vector toxicity contribute to the limited use of antisense oligonucleotides (ASOs) and siRNA as therapeutics. As anthrax toxin (Atx) accesses the cytosol, the purpose of this study was to evaluate the potential of disarmed Atx to deliver either ASOs or siRNA. We hypothesized that this delivery strategy would facilitate improved transfection efficiency while eliminating the toxicity seen for many vectors due to membrane destabilization. Atx complex formation with ASOs or siRNA was achieved *via* the in-frame fusion of either *Saccharomyces cerevisiae* GAL4 or *Homo sapien sapien* PKR (respectively) to a truncation of Atx lethal factor (LFn), which were used with Atx protective antigen (PA). Western immunoblotting confirmed the production of: LFN-GAL4, LFn-PKR and PA which were detected at ~45.9 kDa, ~37 kDa, and ~83 kDa respectively and small angle neutron scattering confirmed the ability of PA to form an annular structure with a radius of gyration of 7.0 ± 1.0 nm when placed in serum. In order to form a complex with LFn-GAL4, ASOs were engineered to contain a double-stranded region, and a cell free *in vitro* translation assay demonstrated that no loss of antisense activity above 30 pmol ASO was evident. The *in vitro* toxicity of both PA:LFn-GAL4:ASO and PA:LFn-PKR:siRNA complexes was low (IC_{50} > 100 μg/mL in HeLa and Vero cells) and subcellular fractionation in conjunction with microscopy confirmed the detection of LFn-GAL4 or LFn-PKR in the cytosol. Syntaxin5 (Synt5) was used as a model target gene to determine pharmacological activity. The PA:LFn-GAL4:ASO complexes had transfection efficiency approximately equivalent to Nucleofection® over a variety of ASO concentrations (24 h post-transfection) and during a 72 h time course. In HeLa cells, at 200 pmol ASO (with PA:LFN-GAL4), 5.4 ± 2.0% Synt5 expression was evident relative to an untreated control after 24 h. Using 200 pmol ASOs, Nucleofection® reduced Synt5 expression to 8.1 ± 2.1% after 24 h. PA:LFn-GAL4:ASO transfection of non- or terminally-differentiated THP-1 cells and Vero cells resulted in 35.2 ± 19.1%, 36.4 ± 1.8% and 22.9 ± 6.9% (respectively) Synt5 expression after treatment with 200 pmol of ASO and demonstrated versatility. Nucleofection® with Stealth RNAi™ siRNA reduced HeLa Synt5 levels to 4.6 ± 6.1% whereas treatment with the PA:LFn-PKR:siRNA resulted in 8.5 ± 3.4% Synt5 expression after 24 h (HeLa cells). These studies report for the first time an ASO and RNAi delivery system based upon protein toxin architecture that is devoid of polycations. This system may utilize regulated membrane back-fusion for the cytosolic delivery of ASOs and siRNA, which would account for the lack of toxicity observed. High delivery efficiency suggests further *in vivo* evaluation is warranted.

Abbreviations: ASOs, antisense oligonucleotides; Atx, anthrax toxin; BME, beta-mercaptoethanol; MTT, 3-(4,5-dimethylthiazol-2-yl)-2,5-diphenyltetrazolium bromide; E7, early 7; EEA1, early endosomal antigen 1; LFn, Atx lethal factor domain I; GFP, Green fluorescent protein; PKR, *Homo sapien sapien* protein kinase-R; HPV, human papilloma virus; ILVs, intraluminal vesicles; LBPA, lysobisphosphatidic acid; LAMP2, lysosome associated membrane protein 2; LF, lethal factor; MVBs, multivesicular bodies; PEI, poly(ethyleneimine); PNS, post-nuclear supernatant; PA, protective antigen; GAL4, *Saccharomyces cerevisiae* galactose metabolism DNA binding protein; SANS, small-angle neutron scattering; (si)RNA, small interfering; Synt5, Syntaxin5; t-GFP, turbo-GFP.

* Corresponding author.
E-mail address: S.C.W.Richardson@Greenwich.ac.uk (S.C.W. Richardson).

[1] These authors contributed equally to this manuscript.

http://dx.doi.org/10.1016/j.jconrel.2015.10.054

1. Introduction

Inefficient cytosolic delivery, suboptimal pharmacokinetics and pharmacodynamics and vector toxicity contribute to the limited application of antisense oligonucleotides (ASOs) and small interfering (si)RNAs as routinely used clinical tools [1,2]. A variety of non-viral delivery systems have been explored in relation to the intracellular delivery of siRNA and ASOs. However, to date, despite three antisense drugs being licensed by the FDA [3,4,5], no ASO intracellular delivery systems have entered into routine clinical use [1,2].

Anthrax toxin (Atx) has evolved to mediate the cytosolic delivery of macromolecules [6] and the attenuation of its intrinsic toxicity using recombinant technology is facile *i.e.* using recombinant PCR to remove Lethal Factor (LF) domains II–IV to give rise to the truncated protein LFn [7]. The translocation of LFn into the cytosol requires *Bacillus anthracis* protective antigen (PA) and has been described [6–10]. This operation requires the association of PA with one of its three known receptors (β1-integrin [11], tumor endothelial marker 8 (TEM8) [12] or capillary morphogenesis gene-2 (CMG-2) [13], which are almost ubiquitously expressed in mammals. PA has been reported to form homoheptamers [6] or homooctamers prior to, or during cell receptor association [14], which are then trafficked onto the limiting membrane of intraluminal vesicles (ILVs) within multivesicular bodies (MVBs) [8,9,10]. A pH-driven PA conformational change results in PA membrane insertion (pre-pore to pore transition) [15] and the translocation of LFn over the ILV limiting membrane, into the lumen of the ILV. A subsequent back-fusion event between the ILV and the limiting membrane of the MBV releases LF(n) into the cytosol [8,9,10]. Given that all of the events culminating in back-fusion and LFn cytosolic release are highly regulated, it may be possible to exploit these trafficking events for not only the transport of peptides into the cytosol [16,17,18] but also the movement of nucleic acids, without the aid of any polycationic condensing agents [19,20,21].

Consequently, the aim of this study was to evaluate the potential of Atx components to deliver ASOs and siRNA to the cytosol without generating the toxicity resulting from non-specific membrane destabilization common to many forms of non-viral delivery technology. A cartoon representing the proposed delivery strategy, and the membrane back-fusion event acting as an "airlock" into the cytosol, is shown (Fig. 1) and is based upon the trafficking of LF [8,9,10]. To this end, ASOs or siRNA was joined to LFn *via* the in-frame fusion of a DNA or RNA binding protein requiring *Saccharomyces cerevisiae* galactose metabolism DNA binding protein (GAL4) (for ASOs) [21] or *Homo sapien sapien* protein kinase-R (PKR) [22] (for RNA) to be fused in frame to LFn and used in conjunction with PA.

For the first time, we report the ability of disarmed Atx to deliver ASOs and siRNA to a variety of primate cell lines (HeLa, THP-1 and Vero) without the aid of any polycationic or lipidic helpers. The PA, LFn-GAL4, LFn-PKR proteins and their complexes with ASO and Stealth RNAi™ siRNA were characterized in relation to structure and general toxicity in Hela and Vero cells *in vitro*. Fluorescence microscopy and subcellular fractionation were used to verify cytosolic entry of LFn-GAL4 and LFn-PKR or their Texas Red®-labeled analogues and the trafficking of PA to lysobisphosphatidic acid (LBPA) positive endocytic vesicles over time. Finally the ability of the disarmed Atx to deliver ASOs and siRNA to a variety of primate cell lines (HeLa, THP-1 and Vero) was studied by measuring the knockdown of Syntaxin5 (Synt5) expression as a model to quantitate pharmacological activity in relation to Nucleofection® (and lipofection) as a benchmark available commercially to anyone wishing to gauge the efficiency of their system in relation to the data reported herein.

2. Materials and methods

2.1. Oligonucleotides

ASOs are described (Table 1) and were supplied by Invitrogen (Paisley, UK). The antisense sequence against Synt5 has previously been published [23]. Synt5 specific Stealth RNAi™ siRNA modified RNA (4392420; Life Technologies, Paisley, UK) was purchased commercially.

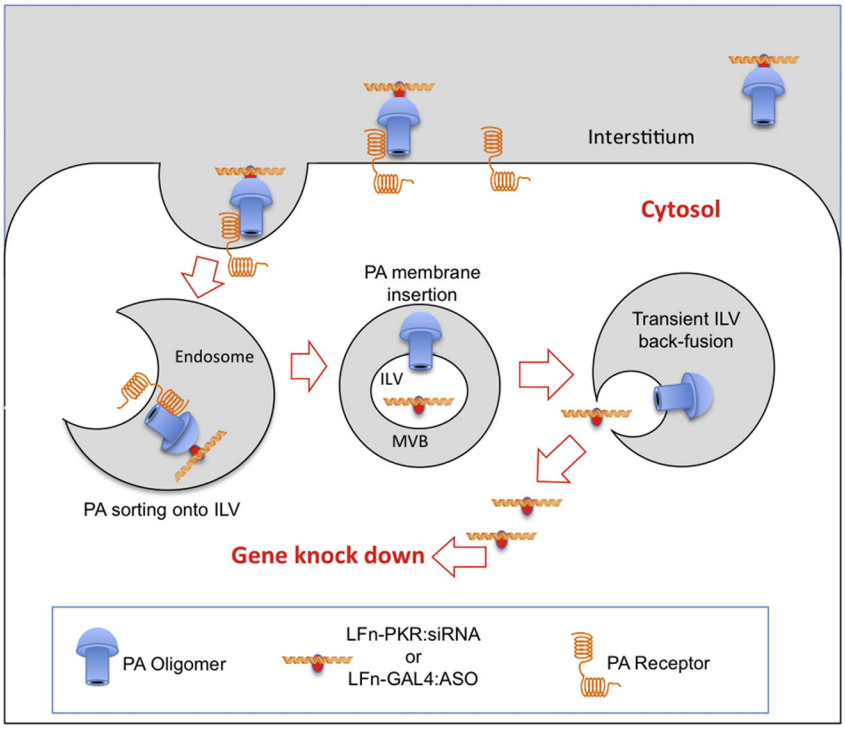

Fig. 1. Exploiting membrane back-fusion for the delivery of ASOs and siRNA. This cartoon is adapted from data describing the cytosolic translocation of LF(n) [6–10]. For the purposes of this study it is used to illustrate the possible route taken to the cytosol by the Atx derived delivery systems described herein *i.e.* PA:LFn-GAL4:ASO or PA:LFn-PKR:siRNA.

Table 1
ASO targets and sequence.

ASO	Target	
Forward	Snyt5	5′-FFZ ZZE ZZZ EZZ EFE EOZ FAT GCA TGC CGG CAT CAG AGC AGC CGG CAT
Reverse	Snyt5	5′-FFZ ZZE ZZZ EZZ EFE EOZ FAT GCA TGC CGG CTG CTC TGA TGC CGG CAT
Forward	tGFP	5′-EEZ EOZ OZZ OFZ OZZ EZZ EEZ ATG CAT GCC GGC TGC TCT GAT GCC GGC AT
Reverse	tGFP	5′-EEZ EOZ OZZ OFZ OZZ EZZ EEZ ATG CCG GCA TCA GAG CAG CCG GCA TGC AT
Forward	tGFP	5′-GGT GCT CTT CAT CTT GTT GGA
Forward	HPV E7	5′-EEZ OEZ OZE OZE FEO ZZZ OZA TGC ATG CCG GCT GCT CTG ATG CCG GCA T
Reverse	HPV E7	5′-EEZ OEZ OZE OZE FEO ZZZ OZA TGC ATG CCG GCA TCA GAG CAG CCG GCA T

After phosphorothioate modification: A = F, T = Z, C = O and G = E.

2.2. Protein production, isolation and enrichment

The DNA sequences coding for the protein LFn-GAL4 and PA83 (based upon GenBank accession numbers: (LFn) AAY15237, (GAL4) Z73604.1, (PA) AAF86457 and AAT98414) have been previously described [21]. LFn-PKR was synthesized by BioBasic Inc., (Ontario, Canada) using the GenBank accession number AAY15237 and NM_002759 (for PKR). The open reading frame coding for LFn-GAL4 or LFn-PKR was sub-cloned into the bacterial expression cassette pET151/D (Invitrogen, Paisley, UK). The addition of a V5 epitope tag and a 6× histidine affinity tag allowed immunodetection and affinity purification from bacterial lysate. LFn-GAL4, LFn-PKR or PA83 were enriched from cultures of *Escherichia coli* with a yield of approximately 2 mg/L using chemically competent *E. coli* BL21*DE3pLys (Invitrogen, Paisley, UK) transformed with 10 ng of plasmid and cultured overnight in 2xYT containing 200 μg/mL ampicillin (Sigma, Dorset, UK) and then grown in 1000 mL of 2xYT at 37 °C and 200 rpm for 3 h. Subsequently, isopropylthio-β-galactoside (Sigma, Dorset, UK) was added to a final concentration of 1 mM and incubated for a further 2 h. Bacterial pellets prepared by centrifugation (6 000×g for 10 min at 4 °C) were lysed using a French Press (Thermo Scientific, Paisley, UK) set to 15 000 psi. Lysates were cleared (18 000 ×*g* for 30 min at 4 °C) and the supernatant passed over a 6× histidine affinity chromatography column (Talon® resin; Clontech, Saint-Germain-en-Laye, France). The 6×His containing proteins were eluted using 150 mM imidazole (Sigma, Dorset, UK) in PBS, in fractions of 1 mL. Protein fractions were analyzed for purity and concentration, pooled, and dialyzed to exhaustion against PBS then filter sterilized (0.22 μm filter). The final protein preparation was evaluated by SDS-PAGE and subjected to Coomassie staining (to determine purity) and Western blot analysis using the antibodies described.

2.3. Protein:nucleic acid complex formation

The hybridization of oligonucleotides with LFn-GAL4 has been described previously [21]. The PA:LFn-GAL4:ASO complex was assembled as follows: first, two partially complementary oligonucleotides, each encoding one strand of a GAL4 recognition sequence, were annealed to form a double-stranded (GAL4) binding sequence with flanking (single-stranded) antisense sequences. Antisense oligonucleotide hybridization was performed by repeatedly (×10) melting (1 min at 94 °C), and re-annealing (1 min at 55 °C), the two partially overlapping oligonucleotides after an initial 2 min step at 94 °C. This ASO hybrid was then introduced to 20 μg/mL LFn-GAL4 and 50 μg/mL PA83 and this left for 30 min at room temperature to self-assemble. The PA:LFn-PKR:siRNA complex was assembled in an identical manner to the PA:LFn-GAL4:ASO complex substituting sterilized LFn-PKR for LFn-GAL4 and the Stealth RNAi™ siRNA specific for Synt5 for the annealed ASOs. Texas Red®-labeling of LFn-GAL4 and LFn-PKR was performed as previously described for bovine serum albumin [24]. Typically less than 5% (w/v) free Texas Red® was found in the salted exchanged preparation. LFn-GFP was produced as previously described [25].

2.4. Cell culture

The culture and passage of HeLa (ATCC: CCL2), Vero (E6; ATCC: CRL-1568) and THP-1 (ATCC: TIB-202) cells were described by the supplier. THP-1 cells were subject to terminal differentiation by adding 320 nM phorbol 12-myristate 13-acetate (Sigma, Dorset, UK) 24 h prior to the transfection experiments. Where undifferentiated THP-1 cells were used the cells were treated as if they were in suspension. Cells were routinely maintained at 37 °C in 5% (v/v) CO_2.

2.5. In vitro toxicity

The PA:LFn-GAL4:ASO and PA:LFn-PRK:siRNA complexes and their components were tested for toxicity in relation to poly(ethyleneimine) (PEI) (Sigma, Dorset, UK) using 3-(4,5-dimethylthiazol-2-yl)-2,5-diphenyltetrazolium bromide (MTT) (Sigma, Dorset, UK). IC_{50} values were calculated using Prism 6.0 (GraphPad software Inc., Ca, USA). This methodology has been previously described [26].

2.6. Transfection experiments

The PA:LFn-GAL4:ASO or PA:LFn-PKR:siRNA complex containing, serum-free cell culture media (2 mL) was added to cells seeded at 5×10^5 cells/well 18 h previously, incubated at 37 °C for 240 min prior to being replaced with complete media. Analysis of target gene expression was performed by removing the cell culture media, washing the cells 3 times in PBS and dissolving the monolayer in 100 μL of Laemmli sample buffer containing 10% (v/v) beta-mercaptoethanol (BME). HeLa cells were subject to Nucleofection®, using a Nucleofector® 2b (Lonza, Slough, UK) and a volume of 0.1 mL. In the instance of HeLa cells, the high efficiency program I-013 was selected and Nucleofection® kit R was used with 5×10^5 cells. The Nucleofection® of undifferentiated THP-1 cells was performed using the high viability Nucleofector® program U-001 and Nucleofector® kit V (Lonza, Slough, UK), as when the high efficiency program (V-001; Lonza, Slough, UK) was used, cell death prevented the acquisition of data. Vero cells were subject to Nucleofection® using program (V-001) and kit V. HPV E7 was detected by Western immunoblotting as before, using an HPV18 E7-specific monoclonal primary antibody (ab100953; AbCam; Cambridge UK, used at a dilution of 1:1000) and an HRP-conjugated anti-mouse secondary (NA931; GE Healthcare; Bucks, UK; used 1:1000). Oligofectamine® (Life Technologies, Paisley, UK) was used with the stated quantity of ASO as per the manufacturer's instructions. Similarly sham-transfection experiments with Lipofectamine® were performed with 1 μg pGST-GFP, a plasmid containing no mammalian promoter [27] and 5 μg of Lipofectamine® (Invitrogen, Paisley, UK) as per the manufacturer's instructions.

2.7. Western blotting and immunodetection

Western blotting was performed using the Mini-PROTEAN® Tetra Cell and electroblotting system (BioRad, Hercules, CA, USA) following the manufacturer's instructions. Typically, 12% (w/v) acrylamide containing resolving gels were used and transfer was conducted at 400 mA for 60 min. All antibodies were diluted into PBS containing 0.01% (v/v) TWEEN20 (Sigma, Dorset, UK) and 5% (w/v) non-fat dried milk (Marvel, Premier Foods plc, St. Albans, UK). Blocking steps were performed for 60 min shaking at 37 °C using the antibody diluting buffer. Antibody hybridizations were performed at 60 min shaking at 37 °C in a volume of 3 mL. Between the blocking steps and after antibody hybridization, three PBS (containing 0.01% (v/v) TWEEN20) washes were performed (5 min at room temperature with gentle shaking).

The final wash prior to autographic detection was conducted with PBS only. Detection was performed using pico-stable ECL reagent (Thermo Scientific, Paisley, UK) and X-ray film (Kodak, Rochester, NY, USA) following the manufacturer's instructions. Exposed X-ray film was developed, scanned and analyzed using NIH ImageJ, before normalizing the expression level of the target gene to that of a housekeeper (early endosomal antigen 1 (EEA1)), detected using a monoclonal anti-EEA1 primary antibody (610456; BD Bioscience; Oxford, UK) at a dilution of 1:1000. As before an anti-mouse HRP-conjugated secondary was used to detect the primary anti-EEA1 antibody. Care was taken to not exceed the dynamic range of the detection system. Synt5 expression was detected using a rabbit polyclonal Synt5-specific primary (13259648; Thermo Scientific; Paisley, UK) and an anti-rabbit-specific, HRP-conjugated secondary antibody (NA934v; GE Healthcare; (Bucks, UK)) diluted 1:1000. The immunodetection of PA was performed using a rabbit anti-PA83 primary antibody (ab13808; AbCam; Cambridge, UK, diluted 1:1000), and an anti-rabbit-HRP-conjugated secondary antibody as before. LFn-GAL4 (or LFN-PKR) was immunodetected using a monoclonal anti-V5 primary antibody (ab13808; AbCam; Cambridge, UK, diluted 1:1000) with an anti-mouse-HPR-conjugated secondary as before. For Western blotting and immunodetection typically 100 ng for recombinant protein was used as a reference.

2.8. SANS and data analysis

Deuterated PA83 protein was grown in 2xYT containing 50% (v/v) deuterium oxide (Sigma, Dorset, UK) and was subject to isolation and purification as before. Proteolytic cleavage was performed using 1 μL trypsin (0.025% (w/v) trypsin and 0.01% (w/v) EDTA) (Invitrogen, Paisley, UK) in PBS per mg of deuterated PA83. The PA digest was left for 20 min at room temperature to produce deuterated PA63. The reaction was stopped by adding an excess of Complete™ EDTA-free protease inhibitor cocktail (Roche, Burgess Hill, UK). The liberated PA20 fragment was removed by affinity chromatography as before. LFn-GFP was added to excess as well as fetal bovine serum (FBS) (Invitrogen, Paisley, UK), to a final concentration of 50% (v/v) FBS, giving a final concentration of 1 mg/mL deuterated PA63. This was in contrast to the deuterated PA63 that was diluted to 1 mg/mL in PBS. Both preparations were placed into separate "banjo" cuvettes (Hellma, Essex, UK). The SANS measurements were performed on the fixed-geometry, time-of-flight LOQ diffractometer (ISIS Spallation Neutron Source, Oxfordshire, UK). All measurements were carried out at 25 °C. Experimental measuring times were approximately 80 min. All scattering data were normalized for the sample transmission and incident wavelength distribution, as well as corrected for instrumental and sample backgrounds using a

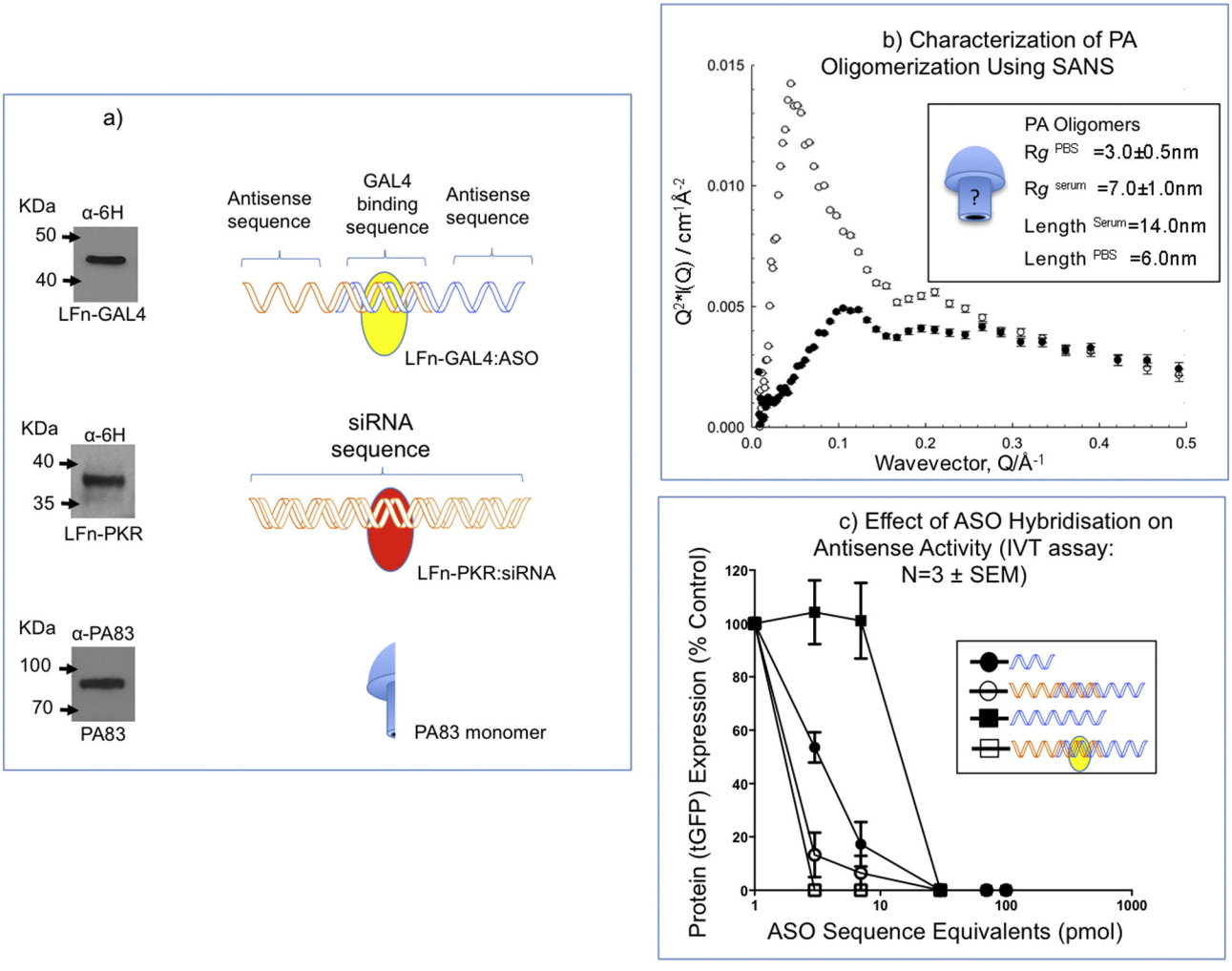

Fig. 2. Characterization of LFn-GAL4 & LFn-PKR, PA83 and ASOs used herein. Here PA:LFn-GAL4 and PA:LFn-PKR components were characterized by both: (i) Western blotting (a, inset) (PA83, LFn-GAL4 and LFn-PKR) and (ii) SANS (PA) (b). Western blotting and immunodetection revealed the enriched proteins to be of the predicted molecular weight. Characterization by SANS was performed by assessing the ability of recombinant, deuterated PA63 (*i.e.* "activated" PA83) to form oligomers in either 50% (v/v) fetal bovine serum (open circles) or PBS (black circles). An IVT kit was used measuring the inhibition of tGFP expression relative to the addition of a negative control (PBS). The inhibition mediated by; a 21mer ASO (closed circle) specific for tGFP, one strand of the hybrid described (closed square), the ASO hybrid described (open circle), and the ASO hybrid described (Fig. 1a) mixed with LFn-GAL4 (open square) are shown (c). For all of the antisense treatments described, equal numbers of antisense sequence were used.

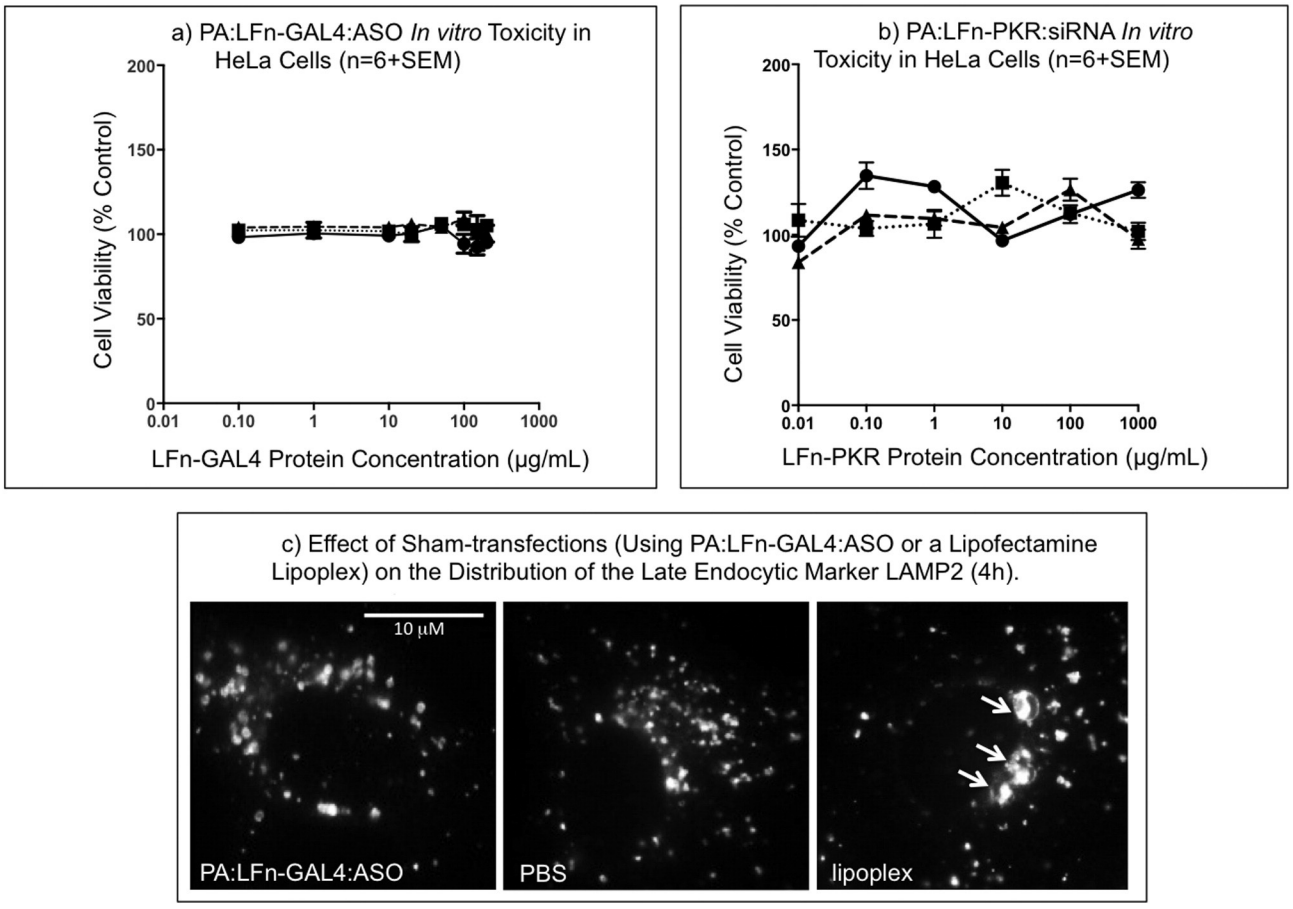

Fig. 3. *In vitro* toxicity. The effects of the PA:LFn-GAL4:ASO upon HeLa cell viability over 24 (circles), 48 (squares) and 72 h (triangles) were recorded using the MTT assay (a). PA:LFn-PRK:siRNA *in vitro* toxicity is also shown (b) and was conducted as previously described (a) substituting LFn-GAL4 for LFn-PKR. Sub-lethal toxicity was investigated using sham transfections (Lipofectamine®), PBS or PA:LFn-GAL4:ASO treated Vero cells. The appearance of hyper-fused, swollen late endocytic structures (arrows) denoted sub-lethal toxicity (c). The concentrations used were those required for robust transfection.

quartz cell containing the appropriate buffer, and for the linearity and efficiency of the detector response. The data were put onto an absolute scale using a well-characterized partially deuterated polystyrene-blend standard sample. The scattering pattern was analyzed as a Guinier representation (the logarithm of the intensity *versus* the square of the wavevector, ln I(Q) *vs.* Q^2), from which a shape-independent radius of gyration was obtained from the initial linear portion of the decay *via* its slope ($-R_g^2/3$). The data describing dPA63 in serum was in agreement with the PA83 derived multimers documented in the protein data bank (PDB accession 1TZN). As various inflexia in this representation of the data were indicative of non-Gaussian statistics, the data was recast in a Kratky plot, namely Q^2. I(Q) *vs.* Q, which removed any Gaussian-like coil (Q^{-2}) dependence.

Table 2
In vitro toxicity after 72 h (IC_{50} (μg/mL; n = 6 ± SEM).

	HeLa cells	Vero cells
25 kDa branched PEI	2.9 ± 0.6	7.3 ± 0.1
0.8 kDa branched PEI	2.4 ± 0.2	7.4 ± 0.3
20 kDa linear PEI	3.0 ± 0.1	6.9 ± 0.5
ASO	100+	100+
PA	100+	100+
LFn-GAL4	100+	100+
LFn-PKR	100+	100+
PA:LFn-GAL4:ASO	100+	100+
PA:LFn-PKR:siRNA	100+	100+

2.9. In vitro translation (IVT) assay

Control reactions were performed using a 1-step human high-yield mini *in vitro* translation (IVT) kit (Thermo Scientific, Paisley, UK) in conjunction with a control plasmid encoding the protein turbo (t)GFP (Evrogen; Cambridge Bioscience, Cambridge, UK), in 5 μL volumes, incubated for 3 h at 30 °C. The expression of tGFP was monitored by Western immunoblotting using a mouse anti-6His monoclonal primary antibody (631212; Clontech, Saint-Germain-en-Laye, France, at a 1:1000 dilution) and an anti-mouse-HPR-conjugated secondary as before. Various ASO compositions (as described) were added to the reaction at the concentrations given at the beginning of the 3 h incubation period.

2.10. Microscopy and subcellular fractionation

Fractionation experiments were seeded at 1×10^6 cells/150 mm^2 dish and two sub-confluent (~90%) dishes were used per treatment. Treatments consisted of 5 mL serum free media containing 50 μg PA protein and 50 μg of either LFn-GAL4 or LFn-PKR (/mL), which was placed under standard incubating conditions. After 4 h the cells were washed 3 times with PBS and scraped into a 100 μL volume of PBS containing 5× Complete™ EDTA-free protease inhibitor cocktail (Roche, Burgess Hill, UK) and lysed by passage through a 21-gauge needle (×10). Whole cells were then removed by centrifugation (600 ×*g* for 1 min. at 4 °C) and a post-nuclear supernatant (PNS) generated by further centrifugation (4000 ×*g* for 2 min. at 4 °C). Membrane (pellet) and cytosol (supernatant) were then separated by subjecting

PNS to sedimentation at 200,000 ×*g* for 60 min at 4 °C. Both the membrane and cytosol fractions were then adjusted to 100 μL total volume using Lamellae sample buffer containing 20% (v/v) BME. The fractions were analyzed using the following primary antibodies: α-LDH (L7016; Sigma; Dorset, UK), as a cytosolic marker, α-V5 (ab9116; AbCam; Cambridge, UK) to detect either LFn-PKR or LFn-GAL4 and an α-transferrin receptor (TfR) primary (612124; BD-Transduction labs; Oxford, UK), was used to detect the presence of the transferrin receptor, a marker for cell membrane. Microscopy was performed after seeding 1×10^5 Vero cells onto a sterile coverslip and incubating the cells overnight in complete media. The following day PA was added to the cells to a final concentration of 50 μg/mL as well as either Texas Red®-labeled LFn-PKR or LFn-GAL4 at a concentration of 50 μg/mL in serum free media. After 4 h the cells were fixed using formalin [24]. Antibodies specific for EEA1 (E41120; BD-Transduction labs; Oxford, UK) were used as a counter immunostain and were used at a dilution of 1:500. EEA1-specific primary antibodies were detected using a 1:500 dilution of Alexa488-conjugated goat anti-mouse specific secondary antibodies (A11001; Invitrogen, Paisley, UK). Sub-lethal toxicity experiments were performed by seeding Vero cells as before and the following day conducting transfection experiments using the preparations as described. After 4 h the cells were fixed using cold methanol [24] and immunostained using an anti- lysosome associated membrane protein 2 (LAMP2) specific antibody at a dilution of 1:10 (H4B4; DHSB, University of Iowa, IA, USA). This primary antibody was detected using a 1:500 dilution of an anti-mouse Texas Red®-labeled secondary (T-862; Invitrogen, Paisley, UK). PA localization to LBPA positive endocytic vesicles was undertaken by pulsing Vero cells with PA (50 μg/mL) with 200 μM Leupeptin 4 or 8 h prior to fixing the cells with 2% formalin (w/v) and then processed as previously described [24]. Immunodetection was performed using both (rabbit) α-PA (ab13808; AbCam; Cambridge) and (mouse) α-LBPA antibodies (clone 6C4, α-LBPA antibody; Merck Millipore, Watford, UK). Texas Red-conjugated anti-rabbit and Alex488-conjugated anti-mouse secondary antibodies were used to visualize both LBPA and PA.

Cells were imaged using an Eclipse 90*i* overhead fluorescent microscope (Nikon, Japan), using a Nikon Digital Camera (DS-Qi1Nc). The objective used in imaging was an oil immersion CFI Plan Apochromat VC 60XN2 (NA 1.4 WD 0.13 mm) (Nikon, Japan).

3. Results

3.1. Characterization of LFn-GAL4 & LFn-PKR, PA83 and ASOs

A cartoon depicting the LFN-GAL4:ASO complex, the LFn-PKR:siRNA complex and the PA monomer are shown (Fig. 2a). Inset are Western blots where LFn-GAL4 (~45.9 kDa), LFn-PKR (~37 kDa) and PA (~83 kDa) were detected at their predicted molecular weights.

Further characterization of the PA component of this system was conducted by SANS, and showed PA63 (*i.e.* activated PA83) oligomerizing in serum (Fig. 2b) [6]. Analysis of the SANS data plotted as a Guinier representation allowed the derivation of shape-independent

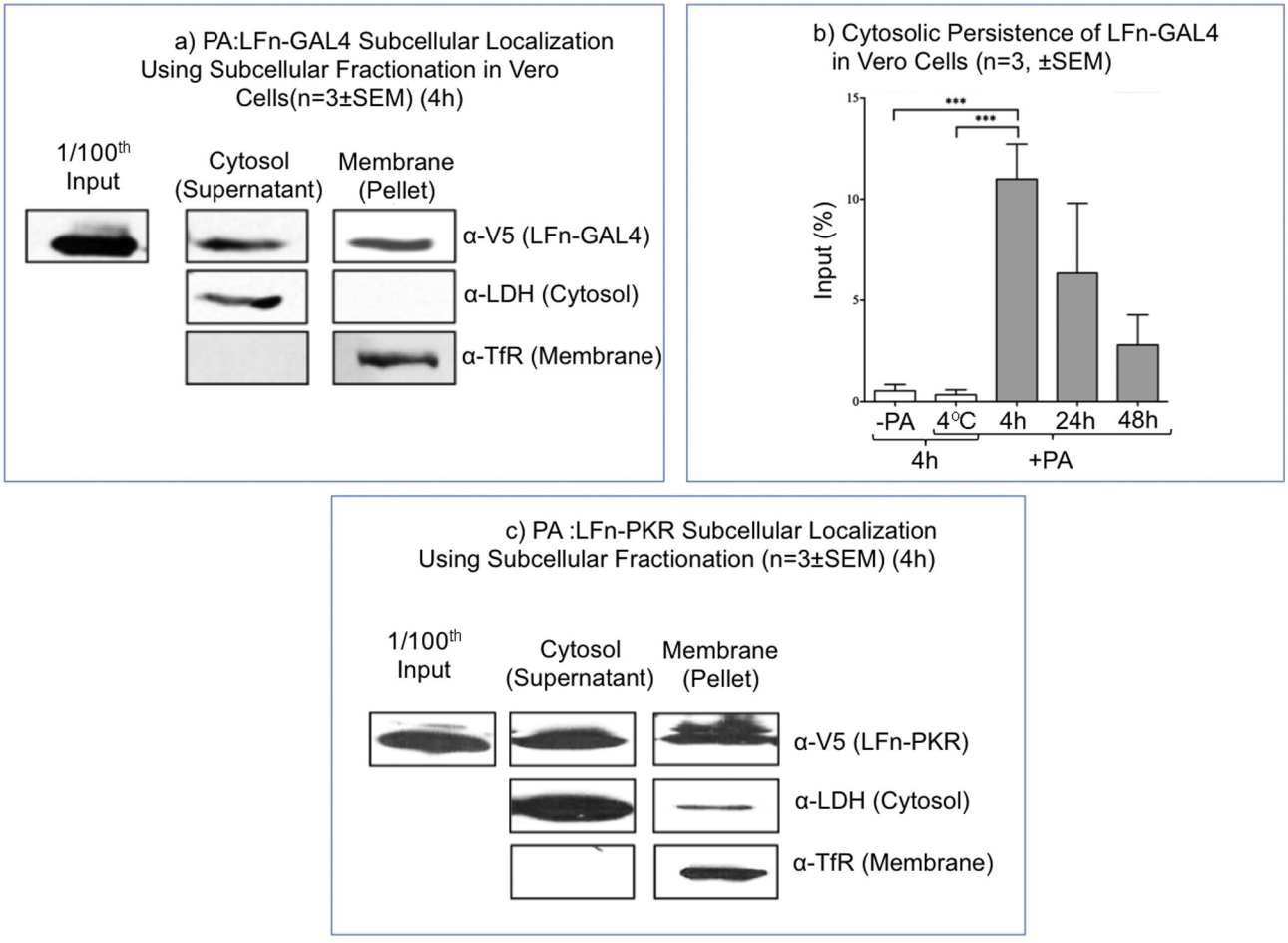

Fig. 4. PA mediated LFn-GAL4 or LFN-PKR cytosolic translocation by subcellular fractionation. Vero subcellular fractionations derived from cells exposed to PA:LFn-GAL4:ASO have been documented and show the detection of LFn-GAL4 (containing an N-terminal V5-epitope) in both the membrane and cytosolic fractions, after 4 h (a). The temporal residence of FLn-GAL4 within the cytosolic fractions derived from this methodology was recorded over time (b). Omitting PA prevented the cytosolic translocation of LFn-GAL4 as did keeping the cells at 0 °C demonstrating specificity. The cytosolic trafficking of PA:LFn-PKR:ASO was also measured by conducting subcellular fractionation (b) as previously described (a), substituting LFn-PKR for LFn-GAL4. LFn-PKR also contained an N-terminal V5-epitope.

radius of gyration measurements which were: $R_g^{PBS} = 3.0 \pm 0.5$ nm and $R_g^{serum} = 7.0 \pm 1.0$ nm (data not shown). The absence of highly extended structure (Q^{-1} dependence), was also demonstrated by the decaying (rather than increasing) background and the almost oscillatory nature of the data was indicative of highly non-Gaussian structures. Peaks present in the Kratky plot resulting from the scattering from dPA63 in PBS and in serum (Fig. 2b) reported peaks shifting to smaller Q (serum), indicating a slightly larger annular structure [28], in agreement with previously published descriptions of PA heptamer [6]. By noting that the peak positions $Q_{max} = 2\pi/L$ correlate to distances L = 14.0 nm in serum and 6.0 nm in PBS, it is likely that in PBS, the majority of the oligomers contain less than 7 members. For reasons of clarity and narration, PA heptamers or octamers have been depicted here (Figs. 1 & 2) as a blue "mushroom". A more concise description of this annular structure has been recently published [6].

Further characterization was conducted by examining the effect of ASO configuration and the presence of LFn-GAL4 upon antisense activity using a cell-free *in vitro* translation assay (1-step human high-yield mini *in vitro* translation (IVT) kit; Thermo Scientific, Paisley, UK) (Fig. 2c). Here, the inhibition of tGFP expression was measured relative to the addition of a negative control (PBS), a positive control (a 21mer ASO specific for tGFP), one strand of the hybrid ASO, the ASO hybrid described, or the hybrid described mixed with LFn-GAL4. Above 30 pmol of ASO, equivocal inhibition was observed between all of the materials tested (Fig. 2c).

3.2. In vitro toxicity

An investigation into the effects of the PA:LFn-GAL4:ASO and PA:LFn-PKR:ASO complex upon HeLa cell viability over 24, 48 and 72 h as measured using the MTT assay [26] was conducted (Fig. 3a & b respectively). The data describe both complexes exerting little toxicity over 72 h *in vitro* relative to PEI (Table 2**).** These data were reinforced morphologically using microscopy (Fig. 3c), examining cells decorated with a primary antibody specific for the late endocytic marker LAMP2 (denoting late endosomes and lysosomes), visualized using an AlexFluor488®-labeled secondary antibody. It is of note that after treatment with PBS or the PA:LFn-GAL4:ASO complex, the majority of LAMP2 positive structures exist as discreet puncta. However, after sham transfection using Lipofectamine®, hyper-fuzed, clustered LAMP2 positive structures (lysosomes) are evident (arrows) which may

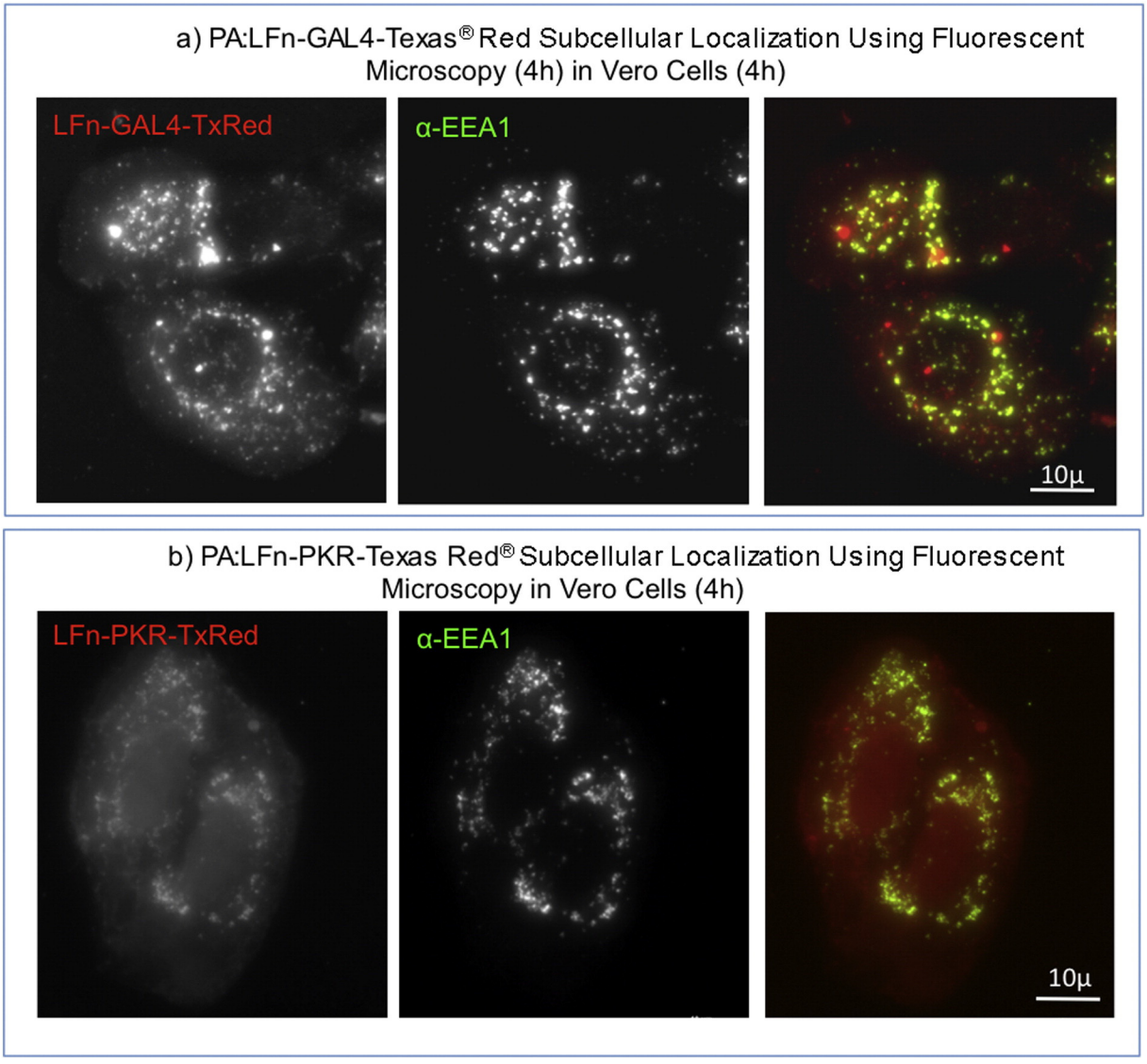

Fig. 5. Evaluation PA mediated LFn-GAL4 or LFN-PKR cytosolic translocation by fluorescence microscopy. The cytosolic translocation of Texas Red®-labeled LFn-GAL4 (a) was recorded as a nebulous haze within both cortical and non-cortical regions of the cell. These cells were counter immunostained with an antibody specific for EEA1, (early endosomes) and after 4 h, Texas Red®-labeled LFn-GAL4 was still detected within EEA1 positive puncta (size bar is 10 μM). Similar observations were made when the experiment was repeated substituting Texas Red®-labeled LFn-GAL4 for Texas Red®-labeled LFn-PKR (b). The localization of PA with LBPA is shown at 4 h and 8 h (c & d respectably) in Vero cells.

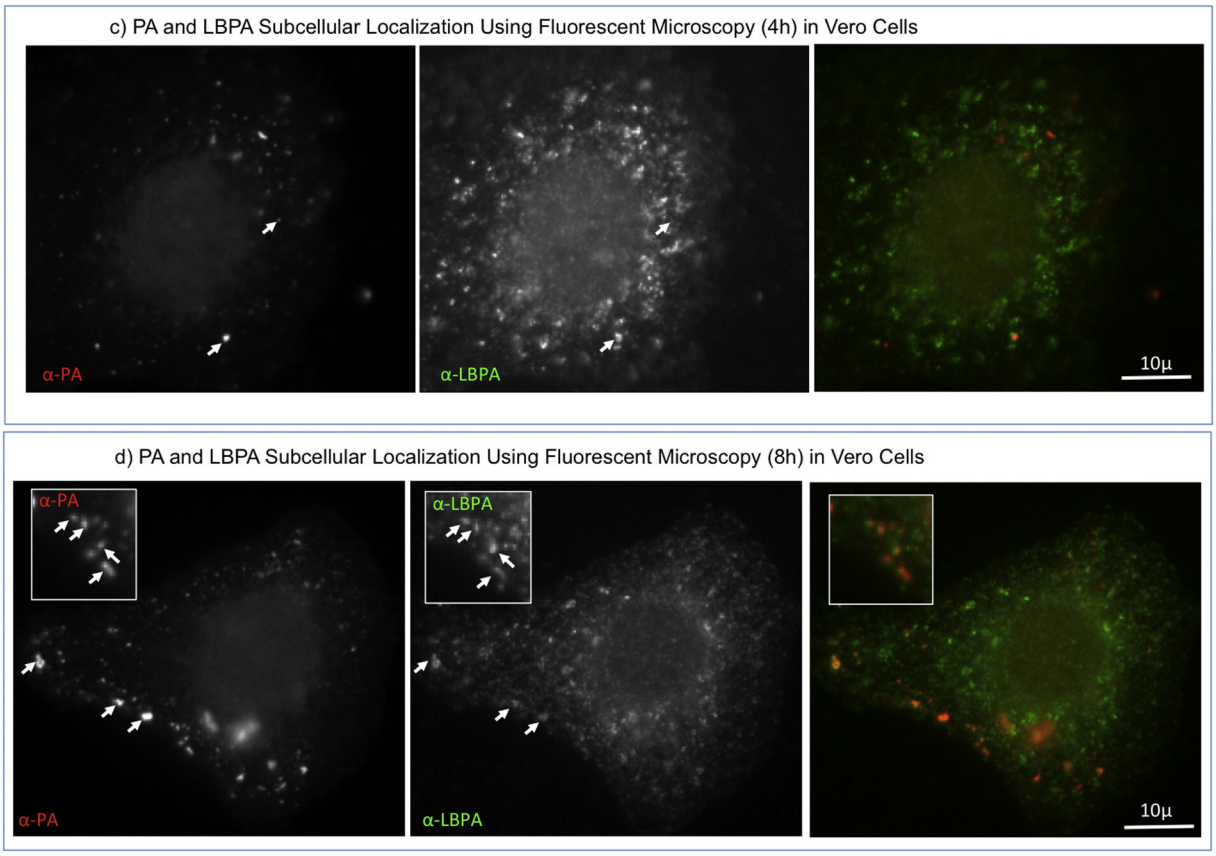

Fig. 5 (*continued*).

indicate a sub-lethal disruption in cellular homeostasis (Fig. 3c). The concentrations chosen were representative of those necessary to perform robust transfection. In an attempt to quantify these microscopic data, 10 randomly selected vesicles were selected from the microtubule-organizing center (the juxtanuclear region with the highest population of vesicles) and their diameters at their widest point measured. The cells exposed to PBS had a mean diameter of 623.5 ± 224.5 nm whereas the cells exposed to PA:LFn-GAL4:ASO had a mean diameter of 688.0 ± 250.7 nm. This was in contrast the cells exposed to the liposectamine lipoplex which had a diameter of 2300.5 ± 1505.2 nm.

3.3. PA mediated LFn-GAL4 or LFn-PKR cytosolic translocation assayed by subcellular fractionation

The activity of the proteinaceous elements of the complexes described was evaluated by assessing the recombinant system's ability to access the cytosol using both subcellular fractionation (Fig. 4) and microscopy (Fig. 5). A 4 h incubation with 50 μg/mL PA resulted in a proportion of a 50 μg/mL dose of LFn-GAL4 (~100 ng, estimated by comparing the V5 signal in the cytosol with the proportion of the input relative to the dose) being detected in an LDH-positive (crude cytosolic) compartment that did not contain any detectable TfR (the membrane marker) (Fig. 4a) as well as in a membrane fraction (containing no LDH). This investigation was continued over time and demonstrated that both PA and a temperature of 37 °C (as opposed to 0 °C) were necessary for the translocation of LFn-GAL4 in the cytosol of Vero cells (after 4 h incubation) and that beyond 4 h, the detectable levels of LFn-GAL4 decline over a 40 h period (Fig. 4b). The ability of the PA:LFn-PKR complex to provide LFn-PKR with access to the cytosol was investigated (Fig. 4c). Although these data show that LDH (the cytosolic marker) was detectable in the membrane fraction, this observation doesn't detract from the observation that similar to LFn-GAL4 (Fig. 4a), LFn-PKR is detectable in an LDH fraction devoid of contamination by the membrane marker (TfR) after an incubation time of 4 h (Fig. 4c).

3.4. Evaluation PA mediated LFn-GAL4 or LFN-PKR cytosolic translocation by fluorescence microscopy

A second string of evidence was tested to reinforce the conclusions drawn from the subcellular fractionation as, if the cytosolic translocation of LFn-GA:4 or LFn-PKR was occurring as described, it might be possible to visualize these phenomena using a single cell assay. After incubation with PA, the visualization of Texas Red®-labeled LFn-GAL4 was documented as an intracellular nebulous haze and within EEA1-positive puncta (*i.e.* early endosomes) in Vero cells (Fig. 5a). It was of note that although a fluid phase marker such as Texas Red®-labeled Dextran or BSA will pass through an EEA1 positive compartment relatively quickly *i.e.* 5–10 min [24], here, Texas Red®-labeled LFn-GAL4 was readily identifiable in an EEA1 positive compartment (*i.e.* co-localizing with EEA1) after 4 h. This may indicate that a fraction of the Texas Red®-labeled LFn-GAL4 remained associated with receptor associated PA.

Common questions raised by this methodology such as the non-specific membrane association of fluorophore and the stability of the Texas Red®-labeling giving rise to false positive data sets were controlled for in the previous experiment, confirming the presence of the protein in the cytosol over a similar time span using not only a different detection system but also a completely separate experimental methodology. The possibility of the release of the fluorophore (*i.e.* the stability of Texas Red®-labeled LFn-GAL4) was addressed in Supplemental Fig. 1, which describes a very different (reticular) staining pattern (relative to Fig. 5) evident when a protein labeled with Texas Red® is chased into the endolysosome without a protease inhibitor. To

repeat the previous observation using Texas Red®-labeled LFn-PKR and PA, a second experiment was undertaken. This resulted in a second form of experimental evidence documenting Texas Red®-LFn-PKR in the cytosol of Vero cells using fluorescence microscopy (Fig. 5b) against an EEA1 counter stain. With morphology similar to Texas Red®-labeled LFn-GAL4 (Fig. 5a), Texas Red®-labeled LFn-PKR was also detected ubiquitously within the cells (Fig. 5b).

Supplemental Fig. 2 further controls for the possibility that the red signal detected in Fig. 5 was autofluorescence, documenting an increase and then decreasing in red signal from Texas Red-labeled LFn-GAL4 over time in live cells. Fig. 5c & d further control of red cytosolic autofluorescence in fixed cells as well as demonstrate that after 4 h a limited amount of co-localization can been seen between a pulse of PA and LBPA (a marker for MVBs and a lipid critical for back-fusion [9]). After an additional 4 h a substantially higher degree of co-localization between PA and LBPA can be observed (Fig. 5d).

3.5. PA:LFn-GAL4:ASO antisense activity against a panel of primate cells

An initial experiment was preformed to evaluate the baseline level of ASO activity in HeLa cells. Here 200 pmol of ASO (or separately siRNA) was added to serum free cell culture media, which was replaced by complete media after 4 h. After 24 h a statistically significant variation in target gene expression was evident relative to a PBS treated control (Supplemental Fig. 3 and supplemental Table 1), where baselines of 71.3% and 69.0% Synt5 expression were recorded for cells treated with only ASO or siRNA respectively.

Having established background levels of ASO transfection (Supplemental Fig. 3 and Supplemental Table 1), the effect of increasing amounts of ASO in concert with static concentrations of PA:LFn-GAL4 was investigated. Antisense activity directed against a target gene (Synt5) was assayed using a HeLa model over 24 h (Fig. 6a). Here, 50 μg of PA and 20 μg of LFn-GAL4 were used/mL at each point measured in a volume of 2 mL. The data was normalized to a housekeeper gene (EEA1) to control for any variability in cell number and show the normalized level of Synt5 expression after treatment of the cells with: (1) media; (2) 200 pmol of nonsense oligonucleotide used with PA:LFn-GAL4; (3) Nucleofection®; (4) the PA:LFn-GAL4; and (5) Oligofectamine®. The PA:LFn-GAL4 when added with ASOs, displayed a pharmacological activity equivalent to Nucleofection® at a variety of ASO concentrations (24 h post-transfection). In HeLa cells, at 200 pmol ASO (+PA:LFn-GAL4), 5.4 ± 2.0% Synt5 expression was recorded relative to an untreated control 24 h after transfection. Using the same number of oligonucleotides and over the same time frame, the Nucleofection® system reduced Synt5 expression to 8.1 ± 2.1% (Fig. 6a). Nucleofection® was performed in 0.1 mL as per the manufacturer's instructions.

The duration of the antisense effect was also investigated in HeLa cells (Fig. 6b) using the same transfection conditions *i.e.* 200 pmol ASO.

Relative to the 0 time point, statistically significant down-regulation of Synt5 was documented using PA:LFn-GAL4:ASO at: 12 h (30.0% ± 14.4) and 24 h (29.5% ± 7.6), and after 12 h (41.6% ± 18), 24 h (31.2% ± 11.6) and 36 h (55.3% ± 8.2) for cells subject to Nucleofection® (Fig. 6b).

The antisense effect previously documented against Synt5 was also directed against an alternate target gene, Human Papilloma Virus serotype 18 Early 7 (HPV18 E7) (Fig. 6c) in an initial attempt to demonstrate both the specificity and versatility of the described transfection system as well as to control for the possibility of the delivery system exerting a non-specific effect, resulting in target gene down regulation. A

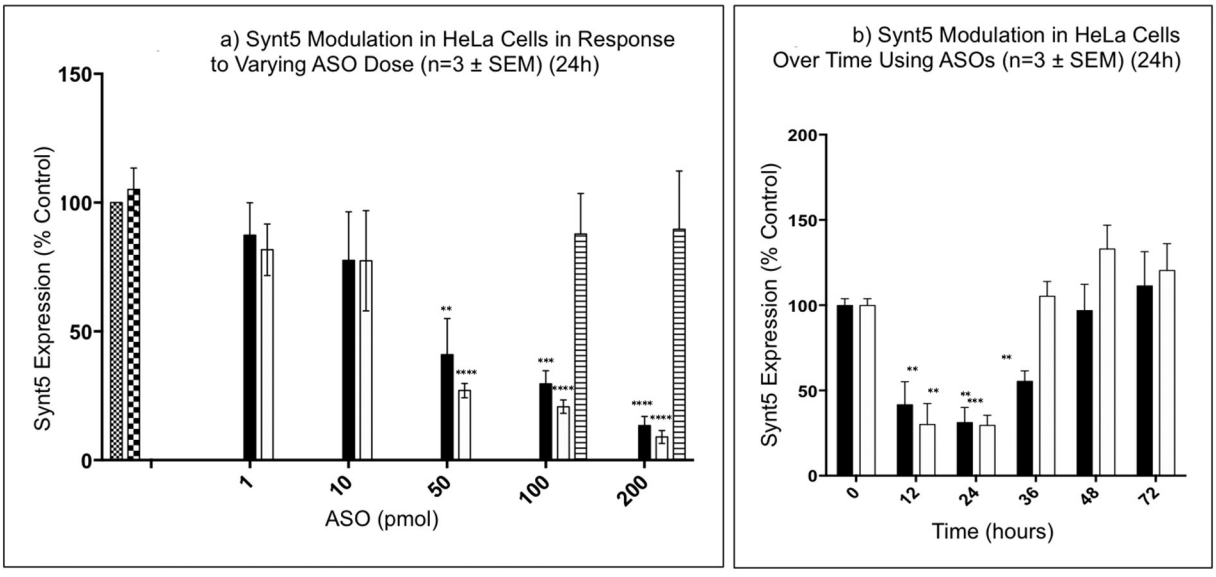

Fig. 6. PA:LFn-GAL4:ASO antisense activity against a panel of primate cells. Transfections were performed in 0.1 mL for Nucleofection® and 2 mL for Oligofectamine® lipoplex and the PA:LFn-GAL4:ASO complex (a) and were normalized to the expression of EEA1. The level of Synt5 expression after: 1) PBS treatment (bars containing small squares); 2) a nonsense oligonucleotide (bars containing large squares); 3) Nucleofection® (solid black bars); 4) the PA:LFn-GAL4:ASO complex (solid white bars); and 5) after treatment with Oligofectamine® (horizontal hatching) are shown. P values showing statistically significant down-regulation of the Synt5 gene relative to the PBS control were (for the PA:LFn-GAL4:ASO complex): 50 pmol ASO (<0.0001), 100 pmol ASO (<0.0001) and 200 pmol of ASO (<0.0001) and for Nucleofection® were: 50 pmol ASO (0.0061), 100 pmol ASO (0.0002) and 200 pmol ASO (<0.0001). The duration of the antisense effect was investigated (b) in HeLa cells where 200 pmol of ASO was used with either PA:LFn-GAL4 or Nucleofection®. Relative to the 0 time point, significant down-regulation of Synt5 was documented (for the PA:LFn-GAL4:ASO complex) at 12 h ($p = 0.0029$) and 24 h ($p = 0.0003$), and at 12 h ($p = 0.0073$), 24 h ($p = 0.0011$) and 36 h ($p = 0.0019$) for cells subject to Nucleofection®. Solid black bars represent cells subject to Nucleofection®, while solid white bars represent cells treated with the PA:LFn-GAL4:ASO complex. The antisense effect documented against Synt5 was also directed against an alternate gene (c) *i.e.* HPV E7 and shows a significant reduction in E7 expression ($p = 0.0104$) after treatment with the PA:LFn-GAL4:ASO complex (solid white bar) relative to PBS treated cells (small squares) (24 h). The effect of PA:LFn:GAL4:ASO complex against undifferentiated THP-1 monocytes was investigated (d). Nucleofection® was attempted using 200 pmol ASO (solid black bar) and 500 pmol (vertical hatched bar) ASO, the latter mediating knock-down ($p = 0.0052$). The PA:LFn-GAL4:ASO complex generated significant Synt5 knock-down using 200 pmol of ASO ($p = 0.0112$). The effect of the PA:LFn-GAL4:ASO complex against differentiated THP-1 macrophages was also investigated (e), and significant down-regulation of Synt5 expression by the PA:LFn-GAL4:ASO complex (clear bar) relative to an untreated control (small squares) was observed ($p = 0.0019$). A significant modulation of Synt5 expression by the PA:LFn-GAL4:ASO complex (clear bar) ($p = 0.0001$) and Nucleofection® (solid black bar) ($p = <0.0001$) relative to the PBS treated control was also recorded in Vero cells (f).

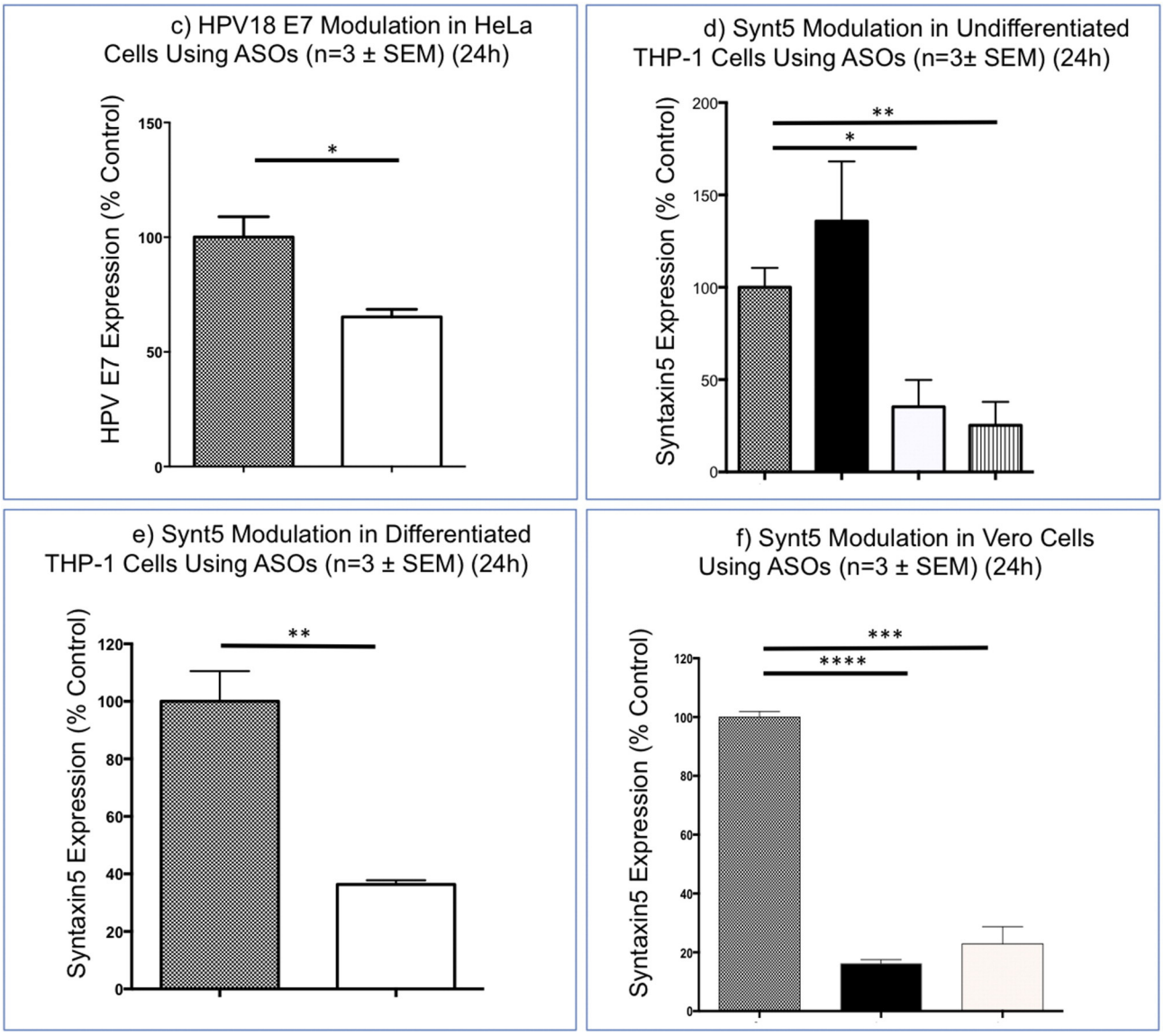

Fig. 6 (*continued*).

statistically significant reduction in E7 expression level was recorded (65.3% ± 4.4) after treatment with the PA:LFn-GAL4:ASO relative to an untreated control after 24 h.

The ability of PA:LFn-GAL4:ASO to down-regulate a target gene in a variety of primate cell lines was also undertaken in order to demonstrate activity in non-HeLa cells. To this end, PA:LFn-GAL4:ASO was directed against Synt5 using undifferentiated THP-1 monocytes (Fig. 6d). Separately, Nucleofection® was also attempted using 200 pmol ASO in the same undifferentiated cells. No Synt5 knock-down was evident after this first attempt at Nucleofection®. When the amount of ASO used was increased to 500 pmol, Synt5 knock-down was evident (25.3% ± 16.8 of Synt5 remained) after 24 h. This was in contrast to the PA:LFn-GAL4:ASO complex, which left a significantly smaller amount of detectable Synt5 (35.2% ± 19.1) after treatment with 200 pmol of ASO after 24 h.

The effect of the Synt5 targeted PA:LFn-GAL4:ASO complex against differentiated THP-1 macrophages was also investigated (Fig. 6e). Here, (35.2% ± 19.1) Synt5 expression was documented after treatment with the PA:LFn-GAL4:ASO complex made with 200 pmol ASO (relative to an untreated control). All attempts at the Nucleofection® of differentiated THP-1 cells resulted in a very high degree of cell death, as would be expected when using this transfection recalcitrant cell line [29]. Consequently, in this instance, no transfection was recorded.

The effect of the PA:LFn-GAL4:ASO complex directed against Synt5 in Vero cells was explored (Fig. 6f). Synt5 expression levels in PA:LFn-GAL4:ASO complex treated cells, relative to an untreated control were recorded (22.9% ± 6.9) as well as the effect of Nucleofection® using Synt5 specific ASOs (16.2% ± 1.7). PA:LFn-GAL4:ASO complex activity in Vero cells demonstrated functionality in a non-human primate species, using a cell line well characterized in our and many other laboratories.

3.6. PA:LFn-PKR:siRNA mediated Synt5 down-regulation

The ability of the PA:LFn-PKR:siRNA complex to deliver pharmacologically active siRNA was examined (Fig. 7). After 24 h; 8.5 ± 3.4% Synt5 expression was recorded after treatment with the PA:LFn-PKR:siRNA complex (containing 200 pmol of Stealth RNAi™ siRNA). This was measured against the Nucleofection® of siRNA using 200 pmol of Stealth RNAi™ siRNA. Treatment with the PA:LFn-PKR:siRNA complex resulted in an almost equivalent level of Synt5 expression of Synt5 relative to Nucleofection® (*i.e.* 4.6 ± 6.1%) using

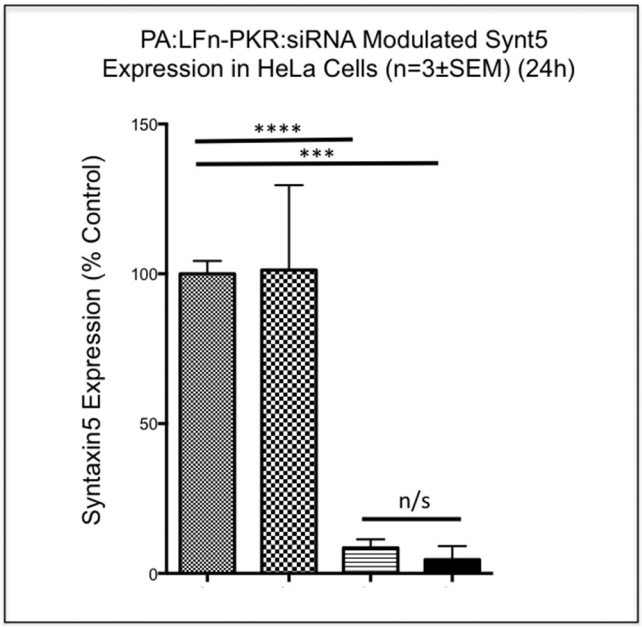

Fig. 7. PA:LFn-PKR:siRNA mediated Synt5 down-regulation. The ability of the PA:LFn-PKR:siRNA complex to deliver Stealth RNAi™ siRNA was investigated and no statistical difference between the ability of the PA:LFn-PKR:siRNA complex to deliver 200 pM siRNA (horizontal hatching) relative to Nucleofection® (black bar) was evident. Both the PA:LFn-PKR:siRNA complex ($p \leq 0.0001$) and Nucleofection® ($p = 0.0001$) showed statistically significant target gene knock-down in HeLa cells after 24 h relative to the PBS treated control (bar containing small boxes). A missense control was also used (bar containing bigger boxes).

the same number of siRNA molecules. To control for siRNA specificity a missense Stealth RNAi™ siRNA was also subject to Nucleofection® and resulted in no measurable reduction in Synt5 levels (Fig. 7).

4. Discussion

The recombinant proteins produced in *E. coli* were detected at the predicted molecular weight when measured by Western immunoblotting and reflect the success of other groups who have performed similar experiments using recombinant protein sequences derived from Atx [16,17,18,25]. The ability of PA to multimerize in serum was confirmed when measured by SANS and the ability of PA:LFn-GAL4 and PA:LFn-PKR to access the cytosol (Figs. 2-5) was confirmed by both subcellular fractionation and microscopy. During the SANS experiments PA63, the "activated" form of PA83, was used in its deuterated form for reasons of contrast and in serum displayed a radius of gyration (R_g) of 7.0 ± 1.0 nm, comparable to the R_g of the heptameric PA pre-pore (PDB accession number 1TZN). Furthermore, the R_g of deuterated PA63 in PBS was 3.0 ± 0.5 nm, and representative of monomeric PA83, predicted to have an R_g of approximately 4.0 nm (PDB accession number 1T6B) (Fig. 2b). The scattering data revealed a non-Gaussian conformation that indicates that deuterated PA63 had assembled into multimeric annular structures in serum, which also reflects the predicted behavior of PA protein from the literature, *i.e.* forms a supramolecular pre-pore approximately 16 × 18 nm (diameter × length) [28]. This observation reinforced the likelihood that the recombinant PA protein would have biological activity similar to its wild type counterpart. These experiments did not have sufficient resolution to differentiate between heptameric and octameric PA oligomers, though it remains unclear whether PA octamerization [14] would aid transfection efficiency in this instance. These data indicate that correctly folded recombinant material had been produced.

Given that oligonucleotide annealing has been documented to initiate at the 3′ end of the oligonucleotide, one concern associated with generating GAL4:ASO complexes (Fig. 2a) was that antisense activity would drop during the use of ASO hybrids (Fig. 2c) or after the association of the hybrid oligonucleotides with LFn-*GAL4* [30]. When tested for antisense activity using an *in vitro* translation assay, beyond 30 pmol of ASO, the antisense activity of the 21mer tGFP-specific ASO, the hybrid ASO and the hybrid in the presence of LFn-GAL4 were equivalent (Fig. 2c). These data may also have value when considering the controlled release profile of this system, as the release of the antisense sequence was not necessary for efficient antisense activity above 30 pmol ASO (Fig. 2c). Little attention was given here to the interaction between GAL4 and double stranded DNA, as this has been well characterized by others [21,30].

Both LFn-GAL4 and LFn-PKR were detected in the cytosol after subcellular fractionation and microscopy. The subcellular fractionation data (Fig. 4) served to reinforce the hypothesis that the signal observed during microscopy was not simply Texas Red®-labeled material binding non-specifically to cell plasma membrane without being internalized, or free Texas Red® released from labeled protein (digested in the endolysosome) staining the cell (Supplemental Fig. 1) or red autofluorescence (Supplemental Fig. 2) [24]. As subcellular fractionation included a control containing no PA as well as an experiment conducted at 0 °C (to demonstrate the specificity of the system) (Fig. 4b), in the interests of brevity, these data are not shown in relation to the microscopy. The localization of PA to an LBPA positive structures adds further credibility to the hypothesis that the recombinant PA produced herein is behaving in a predictable way [9,10], LBPA being a lipid that is critical to the formation of ILVs, to back-fusion and for LF cytosolic translocation [9,10].

Finally, an investigation into the ability of PA:LFn-GAL4:ASO and the PA: LFn-PKR:siRNA complexes to deliver pharmacologically active ASOs and siRNA was undertaken. Modulation of target gene expression recorded in response to the delivery of both ASOs and siRNA were statistically robust, approximately equivalent to Nucleofection® (Figs. 6 & 7) and several logs more potent than lipofection (Fig. 6a) underscoring this system's high efficiency.

Commercially available reference controls (Oligofectamine® and Nucleofection®) were deliberately chosen as a benchmark in order to allow the comparison of the system described herein with other experimental systems, which could also be benchmarked against Oligofectamine® and Nucleofection®. Nucleofection® is a technology routinely used for applications requiring very high efficiency transfection *i.e.* the transfection of libraries and the generation of stable cell lines (the manufacturers claim 99% transfection success) [31]. Consequently, through observing a pharmacological that is comparable to Nucleofection® using the Atx-based system described here, we propose that this new technology also has very high efficiency, though this efficiency may be dependent upon PA receptor expression levels. A second benchmark is documented (Supplemental Fig. 3 &Supplemental Table 1) where the efficiency of the PA:LFn-X systems are compared with both free ASO or siRNA.

Direct comparisons of the systems defined herein with currently relevant delivery technology such as *GalNAc* conjugated siRNA constructs are difficult, as the systems described herein have not yet been tested *in vivo*. *GalNAc* conjugated siRNA have been documented to deliver siRNA to the liver *in vivo* [32] though the mechanism utilized by *GalNAc* to access the cytosol remains unclear. The systems described herein are quite different from this technology, as (1) it is not restricted to tissue expressing the asialoglycoprotein receptor (*i.e.* the liver) and (2) in all probability utilizes a regulated intracellular membrane recycling mechanism (*via* the PA pore) to facilitate endosomal escape (*i.e.* ILV back fusion). As GalNAc contains no pore forming structure, it is unlikely that it utilizes a similar system.

The membrane stress and specificity of PA for LFn were controlled for herein (Supplemental Fig. 4) using cells incubated with both Texas Red®-labeled BSA (10 mg/mL) and PA protein (25 μg/mL), fixed and immunostained for the lysosomal marker LAMP1. Unlike Texas Red®-labeled LFn-GAL4 or Texas Red®-labeled LFn-PKR no cytosolic Texas Red®-labeled BSA was evident. This indirect evidence indicates that ILV back-fusion was, in all probability the most likely system used to

access the cytosol (rather than membrane destabilization). Previously we have demonstrated the release of fluorescent-labeled Gelonin into the cytosol using similar methodology (*i.e.* fluorescence microscopy) to monitor polymer-mediated membrane perturbation and cytosolic cargo transfer [33]. Efforts to investigate the role of ILV back-fusion (more specifically, a dependence on LBPA and ALIX [9] for pharmacological activity of both PA:LFn-GAL4:ASO and PA:LFn-PKR:siRNA) are currently underway.

The pharmacological activity of the Atx-based transfection system described was shown to be reproducible during studies investigating ASO time-dependency and propensity to transfect a selection of primate cell lines (Fig. 6), and (conceptually) *via* the successful delivery of siRNA by PA:LFn-PKR (Fig. 7). Given that the HeLa cells used to document the duration of antisense activity were in an exponential growth phase, it remains possible that the duration of the observed antisense effect (Fig. 6b) may well be extended *in vivo*, though other variables, such as mRNA and protein abundance and half-life, would also need to be considered. Differences in mRNA and protein half-life, abundance and protein-specific biology may also account for the variation in protein knockdown observed when Synt5 is contrasted with HPV18 E7 (Fig. 6a & c).

Relative to the delivery of plasmids, the effective delivery of siRNA and ASOs requires different parameters to be met [34]. Consequently, the use of smaller (relative to a plasmid) pieces of nucleic acid (*i.e.* ASOs) and the absence of polycations [19,20,21] differentiates this work from that of others. In order to condense and conjugate plasmid DNA to disarmed toxins, previous studies have used a polycationic element sometimes described as an "affinity handle" [21]. The lack of a condensing agent to mediate nuclease protection here is countered through the use of chemical modification within the nucleic acid backbone *i.e.* through the use of phosphorothioate ASOs. Similarly, as ASOs and siRNAs were being used, a condensing agent to facilitate the endocytic capture of the PA:LFn-GAL4:ASO or PA:LFn-PKR:siRNA was not necessary. This was important as previous studies [19,20,21] containing polycationic condensing agents *i.e.* poly(Lysine) in conjunction with toxin components may have lent ambiguity to the conclusion that protein architecture alone was responsible for the translocation of the nucleic acid cargo over biological barriers. This is due to the possibility that the toxin-polycation delivery efficiency reported, was being augmented (even indirectly by stressing membrane) by the polycation. Here, this possibility has been controlled for (Supplemental Fig. 4). Condensing agents aside, LFn-GAL4:ASO and LFn-PKR:siRNA size was still contentious as the literature states that the complexes generated herein should be too large to go though the internal lumen of the PA pore, its minimum diameter being approximately 0.6 nm at the phi clamp [6]. In the wild, LF and EF may undergo a molten globular transition, losing higher order structure in order to "ratchet" thorough the internal lumen of the PA pore [6,35]. Given the size of a supramolecular assembly composed of a pair of ASOs and two LFn-GAL4 molecules, (or the LFn-PKR:siRNA equivalent) the data presented herein begins to question the conventional wisdom describing the transition of material over the PA pore, hinting at the possibility of the pore dilating to allow the transit of larger material. Equivalently, it is also possible that the attachment of the ASO or Stealth RNAi™ siRNA to LFn served only to bring nucleic acid into proximal contact with the PA pore interior, facilitating translocation into the lumen of the ILV [36]. Given the diameter of a nucleic acid duplex (~2.0 nm) the DNA would be required to "melt" to pass through the internal lumen of a static PA pore which, like the molten globular transition of LFn-GFP at pH 5.5 may be thermodynamically improbable [25]. Previous studies also failed to address the question of how an interpolyelectrolyte complex (typically 100-200 nm) could "ratchet" through the internal (negatively charged) lumen of the PA (or similar) pore [6,21].

The scope of polycations to interact with membranes [37] mediating toxicity (such as PEI; Table 2), or transfection [38] has been well documented. It was shown here that there was, under the parameters conducive to transfection, very little *in vitro* toxicity when either PA:LFn-GAL4:ASO or PA:LFn-PKR:siRNA were used (Fig. 3), shedding new light upon the "PEG-dilemma" [2,39]. The ramifications of this observation may also stretch beyond toxicity to body distribution and the ability to transfect tissue currently beyond the reach of established non-viral delivery technology [1,2]. The body distribution of the PA protein has been well documented [40,41] and the studies reported here confirmed that PA:LFn-GAL4 and PA:LFn-PKRhave the potential to deliver ASO and siRNA in a variety of different cell types (including monocytes and macrophages (Fig. 6d & e) as efficiently as Nucleofection®. Consequently, experiments will be designed to establish proof of concept in specific disease model *in vivo* in the future.

In relation to loading capacity, assuming PA forms a heptamer [6], three LFn molecules associate with it directly, each forming a dimer with a second LFn-GAL4 molecule binding the ASO hybrid [21,30]. Consequently one discreet $PA_{(7)}$:LFn-$GAL4_{(6)}$:$ASO_{(6)}$ complex has the capacity, when considered as a static unit, to contain 6 antisense sequences. Although the "drug" loading capacity of the PA:LFn-GAL4:ASO complex is undoubtedly less than that of an IPEC, the lack of toxicity, the predictable, regulated nature of membrane translation and lack of a net positive charge (or prevalent hydrophobicity), may serve to counterbalance the efficiency of the PA:LFn-GAL4:ASO complex in relation to the efficiency of the Nucleofection® and lipofection systems reported (Fig. 6). The PA pore may also be able to sustain the delivery of LFn-fusion molecules over time. Efforts are currently underway to quantify how many cytosolic ASO molecules can be detected as a function of delivery in relation to an observed pharmacological effect. This information may be critical when considering the variance of PA receptor density and type in relation to determining the delivery efficiency necessary to treat a specific pathology. Once target mRNA abundance and protein half-life are considered in the light of delivery efficiency, informed decisions about dose may be possible, further reducing unwanted off-target effects due to an excess of "drug". Ultimately, this approach may also allow the precise control over the level of modulation exerted over target gene expression, in a given cell, tissue type or person.

In contrast to LFn, PA has been documented as not being particularly immunogenic in Humans [42]. If repeat dosing is required, immunogenicity may be something that needs to be addressed, but is, for the time being, beyond the remit of this study. If immunogenicity does become a problem, there are potentially several ways of dealing with it without compromising the efficacy of the existing anthrax vaccines (that also contain PA and LF) [42]. One possible solution may be to PEGylate assemblies of PA:LFn-X:ASO/siRNA.

5. Conclusion

The novel antisense and siRNA delivery technology described displays high transfection efficiency and little toxicity *in vitro*. As this cytosolic delivery platform is a departure from conventional charged or hydrophobic, non-viral drug delivery technology, it is also possible that it may not be subject to many of the limitations that have thus far prevented non-viral drug delivery technology from translating into routinely used clinical tools.

Supplementary data to this article can be found online at http://dx.doi.org/10.1016/j.jconrel.2015.10.054.

Acknowledgments

S.C.W.R. and P.C.G. would like to thank the Science and Technology Funding Council (STFC) for their support, funding the neutron scattering work through awards: RB1220030 and RB1320038, to P.C.G. and S.C.W.R., respectively. P.D.R.D., T.R.S., S.A.S., M.P., C.-K.T. and A.S.G. would like to thank The University of Greenwich for funding. S.C.W.R. would like to thank GUEL for supporting this project. Prof. Stephen Leppla (National Institute of Allergy and Infectious Diseases, USA) is

also thanked for the kind gift of a LF encoding plasmid. S.C.W.R would like to thank Prof. Ruth Duncan for critically reading this manuscript.

References

[1] H. Yin, et al., Non-viral vectors for gene based therapy, Nat. Rev. Genet. 15 (2014) 541–555, http://dx.doi.org/10.1038/nrg3763.

[2] O.M. Merkel, T. Kissel, Quo vadis polyplex? J. Control. Release 190 (2014) 415–423, http://dx.doi.org/10.1016/j.jconrel.2014.06.009.

[3] R. Geary, et al., Fomivirsen: clinical pharmacology and potential drug interactions, Clin. Pharmacokinet. 41 (4) (2002) 255–260.

[4] I. Marafini, et al., Antisense approach to inflammatory bowel disease: prospects and challenges, Drugs 75 (7) (2015) 723–730, http://dx.doi.org/10.1007/s40265-015-0391-0.

[5] D. Rader, J. Kastelein, Lomitapide and mipomersen: two first-in-class drugs for reducing low-density lipoprotein cholesterol in patients with homozygous familial hypercholesterolemia, Circulation 129 (9) (2014) 1022–1032, http://dx.doi.org/10.1161/circulationaha.113.001292.

[6] J. Jiang, et al., Atomic structure of anthrax protective antigen pore elucidates toxin translocation, Nature 521 (2015) 545–549, http://dx.doi.org/10.1038/nature14247.

[7] N. Aurora, S.H. Leppla, Residues 1–254 of anthrax toxin lethal factor are sufficient to cause cellular uptake of fused polypeptides, J. Biol. Chem. 268 (1993) 3334–3341.

[8] T. Falguieres, et al., Molecular assemblies and membrane domains in multivesicular endosome dynamics, Exp. Cell Res. 315 (2009) 1567–1573, http://dx.doi.org/10.1016/j.yexcr.2008.12.006.

[9] Abrami L., et al., Membrane insertion of anthrax protective antigen and cytoplasmic delivery of lethal factor occur at different stages of the endocytic pathway. J. Cell Biol., 66(5): 645–651, (2004). doi/http://dx.doi.org/10.1083/jcb.200312072.

[10] J. Gruenberg, F.G. van der Goot, Mechanisms of pathogen entry through the endosomal compartments, Nat. Rev. Mol. Cell Biol. 7 (7) (2006) 495–504, http://dx.doi.org/10.1038/nrm1959.

[11] M. Martchenko, S.-Y. Jeonga, S.N. Cohen, Heterodimeric integrin complexes containing β1-integrin promote internalization and lethality of anthrax toxin, Proc. Natl. Acad. Sci. U. S. A. 107 (2010) 15583–15588, http://dx.doi.org/10.1073/pnas.1010145107.

[12] S. Liu, S.H. Leppla, Cell surface tumor endothelium marker 8 cytoplasmic tail-independent anthrax toxin binding, proteolytic processing, oligomer formation, and internalization, J. Biol. Chem. 287 (2003) 5227–5234.

[13] S. Liu, et al., Capillary morphogenesis protein-2 is the major receptor mediating lethality of anthrax toxin in vivo, Proc. Natl. Acad. Sci. U. S. A. 106 (2009) 12424–12429, http://dx.doi.org/10.1073/pnas.0905409106.

[14] A.F. Kintzer, et al., The protective antigen component of anthrax toxin forms functional octameric complexes, J. Mol. Biol. 392 (2009) 614–629, http://dx.doi.org/10.1016/j.jmb.2009.07.037.

[15] M. Qadan, et al., Membrane insertion by anthrax protective antigen in cultured cells, Mol. Cell. Biol. 25 (13) (2005) 5492–5498.

[16] W.P. Verdurmen, M. Luginbühl, A. Honegger, A. Plückthun, Efficient cell-specific uptake of binding proteins into the cytoplasm through engineered modular transport systems, J. Control. Release 200 (2015) 13–22, http://dx.doi.org/10.1016/j.jconrel.2014.12.019.

[17] X. Liao, et al., Delivery of antibody mimics into mammalian cells via anthrax toxin protective antigen, ChemBioChem 15 (2014) 2458–2466, http://dx.doi.org/10.1002/cbic.201402290.

[18] D.E. Peters, et al., Comparative toxicity and efficacy of engineered anthrax lethal toxin variants with broad anti-tumor activities, Toxicol. Appl. Pharmacol. 279 (2014) 220–229, http://dx.doi.org/10.1016/j.taap.2014.06.010.

[19] L.B. Barrett, et al., CTb targeted non-viral cDNA delivery enhances transgene expression in neurons, J. Gene Med. 6 (4) (2004) 429–438.

[20] J. Fominaya, W.W. Target, D.N.A. Cell-specific, Transfer mediated by a chimeric multidomain protein, J. Biol. Chem. 271 (18) (1996) 10560–10568.

[21] R. Gaur, P. Gupta, A. Goyal, W. Wels, Y. Singh, Delivery of nucleic acid into mammalian cells by anthrax toxin, Biochem. Biophys. Res. Commun. 297 (2002) 1121–1127.

[22] H.J. Stunden, E. Latz, PKR stirs up inflammasomes, Cell Res. 23 (2) (2013) 168–170, http://dx.doi.org/10.1038/cr.2012.125.

[23] K. Suga, et al., RNA interference-mediated silencing of the syntaxin 5 gene induces Golgi fragmentation but capable of transporting vesicles, FEBS Lett. 579 (20) (2005) 4226–4234.

[24] S.C. Richardson, et al., The use of fluorescence microscopy to define polymer localization to the late endocytic compartments in cells that are targets for drug delivery, J. Control. Release 127 (1) (2008) 1–11, http://dx.doi.org/10.1016/j.jconrel.2007.12.015.

[25] I. Zornetta, et al., Imaging the cell entry of the anthrax oedema and lethal toxins with fluorescent protein chimeras, Cell. Microbiol. 12 (2010) 1435–1445, http://dx.doi.org/10.1111/j.1462-5822.2010.01480.x.

[26] S.C. Richardson, et al., Potential of low molecular mass chitosan as a DNA delivery system: biocompatibility, body distribution and ability to complex and protect DNA, Int. J. Pharm. 178 (2) (1999) 231–243.

[27] M.W. Pettit, et al., Construction and physiochemical characterization of a multi-composite, potential oral vaccine delivery system (VDS), Int. J. Pharm. 468 (1–2) (2014) 264–271, http://dx.doi.org/10.1016/j.ijpharm.2014.03.046.

[28] V. Receveur-Brechot, D. Durand, How random are intrinsically disordered proteins? A small angle scattering perspective, Curr. Protein Pept. Sci. 13 (2012) 55–75, http://dx.doi.org/10.2174/138920312799277901.

[29] M.B. Maeß, et al., Optimization of the transfection of human THP-1 macrophages by application of Nunc UpCell technology, Anal. Biochem. 479 (2015) 40–42, http://dx.doi.org/10.1016/j.ab.2014.12.023.

[30] T. Pan, J.E. Coleman, Structure and function of the Zn(II) binding site with in the DNA-binding domain of the GAL4 transcription factor, PNAS 86 (1989) 3145–3149.

[31] http://www.lonza.com/products-services/bio-research/transfection/nucleofector-technology.aspx

[32] Nair, et al., Multivalent N-acetylgalactosamine-conjugated siRNA localizes in hepatocytes and elicits robust RNAi-mediated gene silencing, JACS 136 (2014) 16958–16961.

[33] Richardson, S. C. W., Pattrick, N. G., Lavignac, N., Ferruti, P., & Duncan, R. (2010). Intracellular fate of bioresponsive poly(amidoamine)s in vitro and in vivo. J. Control. Release, 142(1), 78–88. doi.org/http://dx.doi.org/10.1016/j.jconrel.2009.09.025.

[34] C. Scholz, E. Wagner, Therapeutic plasmid DNA versus siRNA delivery: common and different tasks for synthetic carriers, J. Control. Release 161 (2012) 554–565, http://dx.doi.org/10.1016/j.jconrel.2011.11.014.

[35] B.A. Krantz, et al., Acid-induced unfolding of the amino-terminal domains of the lethal and edema factors of anthrax toxin, J. Mol. Biol. 344 (3) (2004) 739–756.

[36] D.G. Wright, et al., Effective delivery of antisense peptide nucleic acid oligomers into cells by anthrax protective antigen, Biochem. Biophys. Res. Commun. 376 (2008) 200–205, http://dx.doi.org/10.1016/j.bbrc.2008.08.124.

[37] Y. Marikovsky, D. Danon, A. Katchalsky, Agglutination by polylysine of young and old red blood cells, Biochim. Biophys. Acta 124 (1966) 154–159.

[38] O. Boussif, et al., A versatile vector for gene and oligonucleotide transfer into cells in culture and in vivo: polyethyleneimine, Proc. Natl. Acad. Sci. U. S. A. 92 (1995) 7297-7230.

[39] T. Liu, B. Thierry, A solution to the PEG dilemma: efficient bioconjugation of large gold nanoparticles for biodiagnostic applications using mixed layers, Langmuir 28 (44) (2012) 15634–15642, http://dx.doi.org/10.1021/la301390u.

[40] M. Moayeri, et al., Anthrax protective antigen cleavage and clearance from the blood of mice and rats, Infect. Immun. 75 (2007) 5175–5184.

[41] E. Dadachova, et al., *In vitro* evaluation, biodistribution and scintigraphic imaging in mice of radiolabeled anthrax toxins, Nucl. Med. Biol. 37 (2009) 755–761, http://dx.doi.org/10.1016/j.nucmedbio.2008.07.001.

[42] L.W. Baillie, et al., An anthrax subunit vaccine candidate based on protective regions of *Bacillus anthracis* protective antigen and lethal factor, Vaccine 28 (2010) 6740–6748.

[43] Dyer, P. D. R., Kotha, A. K., Pettit, M. W., & Richardson, S. C. W. Imaging select Mammalian organelles using fluorescent microscopy: application to drug delivery. Methods Mol. Biol. (Clifton, N.J.), 991, 195–209. (2013). doi.org/http://dx.doi.org/10.1007/978-1-62703-336-7_19.